Supplementary Information

The Impacts of Heterogeneous Constructing on the Low- and High-Index Facets of Cu_2O on the Catalytic Performance and Reconstruction in Electrochemical CO_2 Reduction Reaction

Jiaxing Guo[a], Haiqiang Mu[a], Zhenli Lv[a], Guorui Ma[a], Zhiyu Zheng[a], Jin Zhang[c],

Feng Li[a,b] *, Jing Li[a]*

[a] State Key Laboratory of High-efficiency Coal Utilization and Green Chemical Engineering, School of Chemistry and Chemical Engineering, Ningxia University, Yinchuan, Ningxia, 750021, P. R. China.

[b] Liupanshan Laboratory, Yinchuan 750021, Ningxia, China.

[c] Analysis and Testing Center, Ningxia University, Yinchuan, Ningxia, 750021, P. R. China.

* Corresponding author.

E-mail: jingli18@nxu.edu.cn (Jing Li), fengli@nxu.edu.cn (Feng Li)

Detailed calculation process of Faraday efficiency

The FE calculation followed established protocols:

$$FE_g = \frac{Q_g}{Q_{total}} \times 100\% = \frac{1.67 \times 10^{-8} \times F \times x_g \times v_{CO_2} \times K}{i_{total} \times V_m} \times 100\%$$

$$= \frac{6.56 \times 10^{-5} \times x_g \times v}{i_{total}}$$

where F is the Faraday constant (96485 C mol^{-1}), x_g is the target product concentration (ppm), υco_2 is the CO_2 flow rate (mL min^{-1}) at the outlet of the electrolytic cell, K is the number of electrons transferred corresponding to different products, i_{total} is the total current (mA) in the reaction process, and V_m is the molar volume of the gas (V_m=24.5L mol^{-1} at room temperature and pressure)

$$FE_l = \frac{F \cdot c_l \cdot V \cdot n}{Q_{total}}$$

Where FE_l is the Faraday efficiency for liquid products, c_l is the concentration of liquid product detected from 1H NMR (mol L^{-1}), V is the electrolyte volume in cathode chamber (L), Q_{total} is total electric charge accumulated in electrolysis (C).

Theoretical calculations

The first-principles density functional theory (DFT) calculations were performed via Vienna abinitio simulation package (VASP) from the website (https://www.materialsproject.org/materials/mp-990448/#).

In order to obtain the accurate free energy of CO dimerization reaction, the calculations were performed using the hybrid functional as proposed by PBE interactions are represented using the projector augmented wave (PAW) potential, and the Kohn-Sham one-electron valence states were expanded on the basis of plane waves with a cutoff energy of 400 eV. The Hellmann-Feynman forces convergence criterion was set as less than 0.05 eV $Å^{-1}$, the K-point of 2×2×1 was used for the optimization of Cu_2O and S-doped Cu_2O surface (332), Cu_2S clusters on the Cu_2O surface of 100, 111 and 332, the atomic layer with the thicknesses about 3.0-15.0 Å is anchored.

The zero point energy (ZPE) correction was performed referring to the approaches previously reported. In the DFT process, we calculated the Gibbs free energy according to the equations as follow:

$$G^0=E_{DFT}+ZPE-TS^0$$

Where G^0 is the Gibbs free energy, E_{DFT} is total free energy, ZPE is the vibration energy; TS^0 is the entropy change (T = 298.15 K).

In situ ATR-FTIR spectroscopy measurements

In situ attenuated total reflection Fourier transform infrared (in situ ATR-FTIR) spectroscopy was carried out on a FT-IR Spectrometer (INVENIO, Bruker) equipped with a liquid nitrogen cooled LN-MCT detector, with a resolution of 4 cm^{-1}. The ATR-FTIR measurement was carried by equipping a micro ATR attachment containing a Si crystal

allowing small-area sample measurement. The s-Cu_2O@Cu_2S dropping on an Au thin films sputtered Si internal reflection element served as the cathode/working electrode. An Ag/AgCl (BASI) reference electrode in 3 M NaCl solution was used as the reference electrode, while the counter electrode was a Pt. The spectrometer and sample compartment were purged with nitrogen (5.0 grade) for 30 min to remove atmospheric water vapor and CO_2. The spectroelectrochemical cell was rinsed thoroughly with ultrapure water and then a background spectrum was collected in CO_2-saturated 0.5 M $KHCO_3$ under Open circuit potential. Then the spectra were collected by potentiostatic electrolysis for 1min.

In-situ XRD measurements

In-situ XRD were conducted in a custom-made cell with catalyst deposited carbon paper (Toray, H60), Ag/AgCl and Pt wire as the working electrode, reference electrode and counter electrode, respectively. Kapton membrane was covered on the cell for seal. The electrochemical measurement was realized by the electrochemical station and the applied potential was held at -0.82 V vs. RHE. Each XRD pattern was acquired at a certain time.

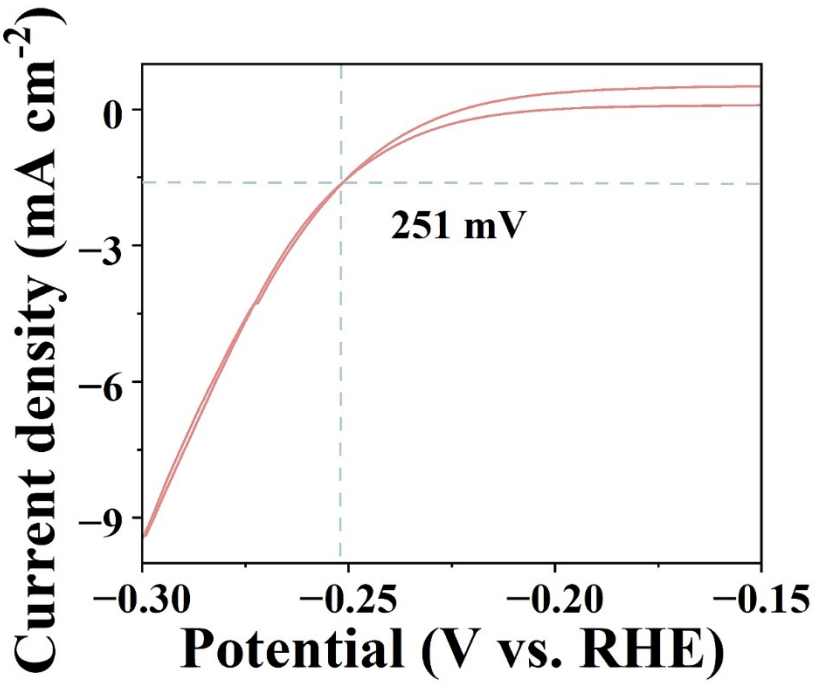

Fig. S1 Calibration of Ag/AgCl reference electrode with respect to RHE in 0.5 M H_2SO_4 at 2 mV s^{-1} scan rate.

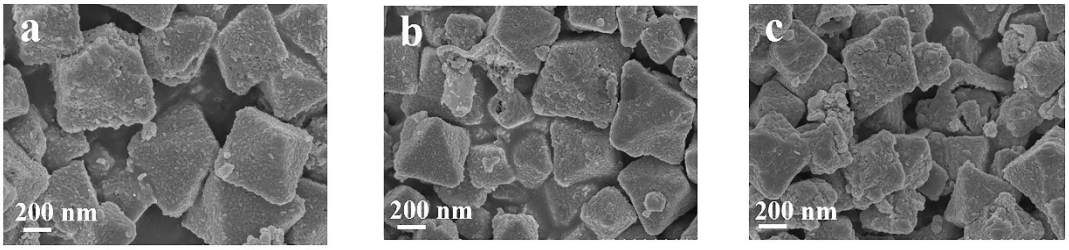

Fig. S2 SEM images of a) s-Cu_2O@$Cu_2S_{1:1.5}$, b) s-Cu_2O@$Cu_2S_{1:1.8}$ and c) s-Cu_2O@$Cu_2S_{1:2}$.

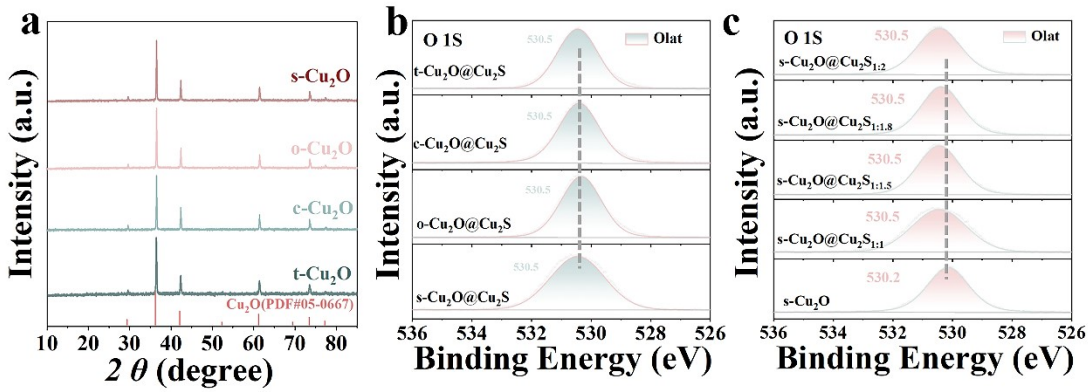

Fig. S3 XRD patterns of various morphologies of (a) Cu_2O with various structures samples. XPS spectra of O 1s collected from (b) Cu_2O@Cu_2S with various morphologies and (c) s-Cu_2O@Cu_2S with varying sulfidation layer thicknesses.

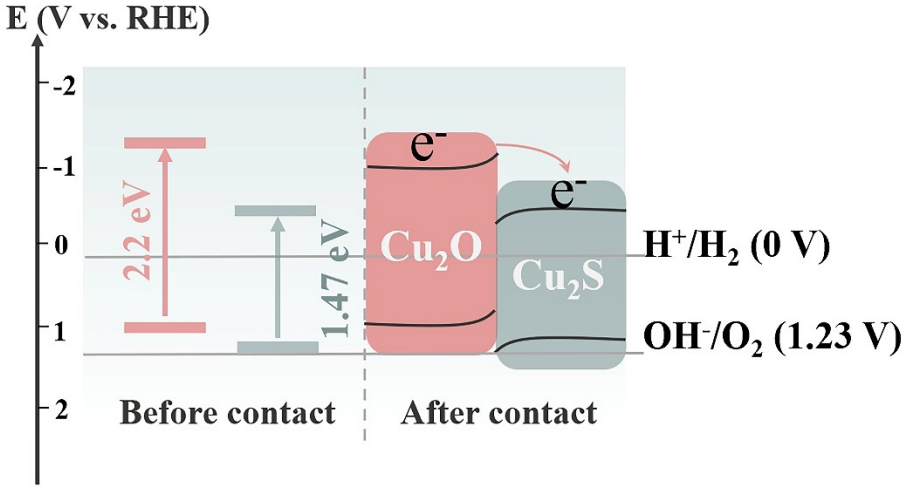

Figure S4. Schematic diagram of energy band structure for s-Cu_2O@Cu_2S.

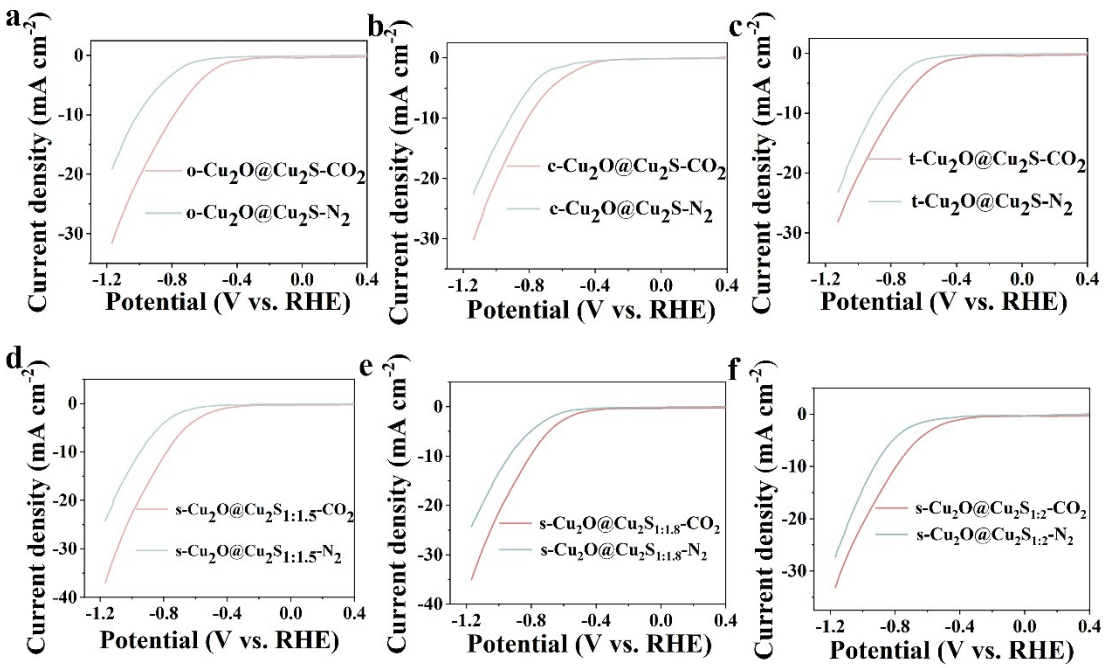

Fig. S5 LSV of (a-c) $Cu_2O@Cu_2S$ with various structures and (d-f) s-$Cu_2O@Cu_2S$ with varying sulfidation layer thicknesses samples saturated with a 0.5 M $KHCO_3$ aqueous solution containing CO_2 and N_2.

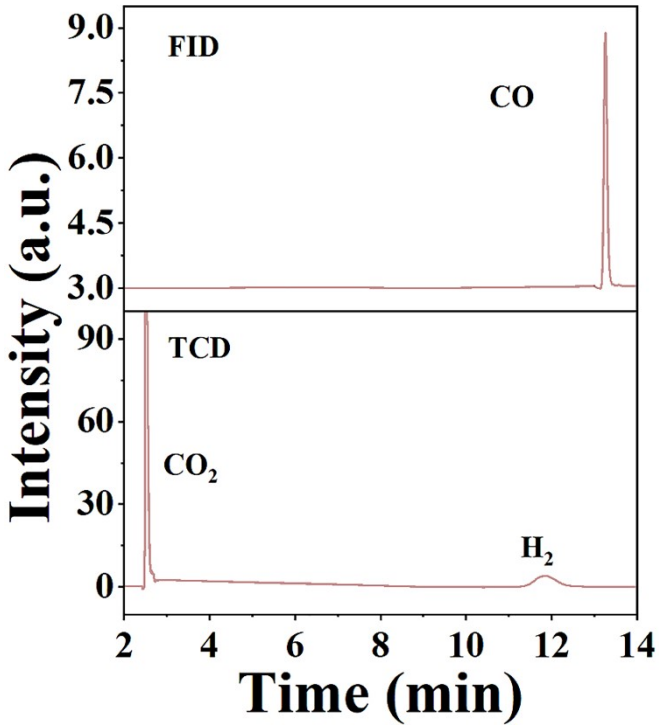

Fig. S6 Representative GC spectra of the gaseous products after electrolysis at - 0.62 V vs. RHE using s-Cu_2O@Cu_2S as the catalyst in a CO_2 -saturated 0.5 M $KHCO_3$ electrolyte solution.

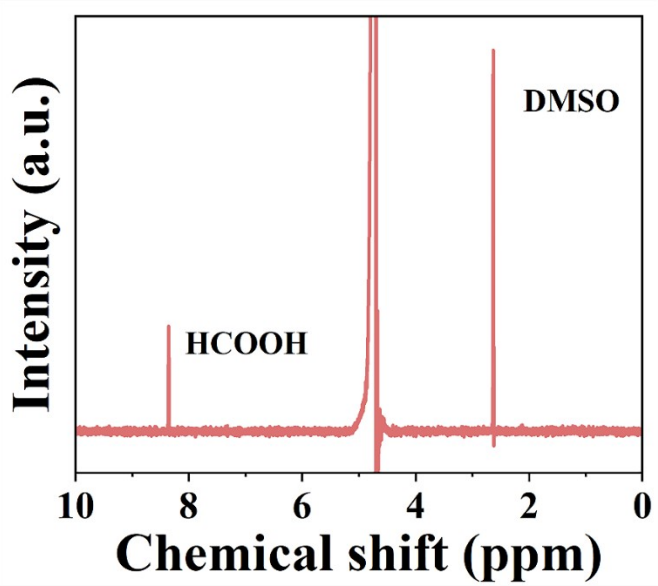

Fig. S7 Representative 1H NMR spectra of the solutions after electrolysis with 30 C charge at -0.62 V vs. RHE for s-Cu_2O@Cu_2S material in a CO_2-saturated 0.5 M $KHCO_3$ electrolyte. DMSO is added as an internal standard to quantify HCOOH.

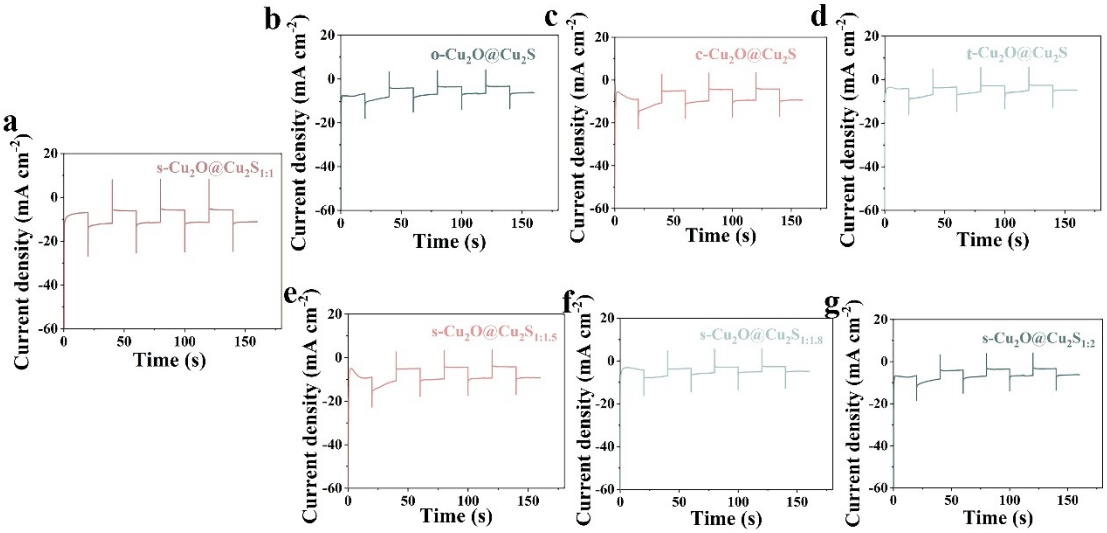

Fig. S8 The function of transient current density with time in the range of −0.5 to −0.6 V vs. RHE of $Cu_2O@Cu_2S$ with different exposed crystal facets and sulfidation layer thicknesses samples.

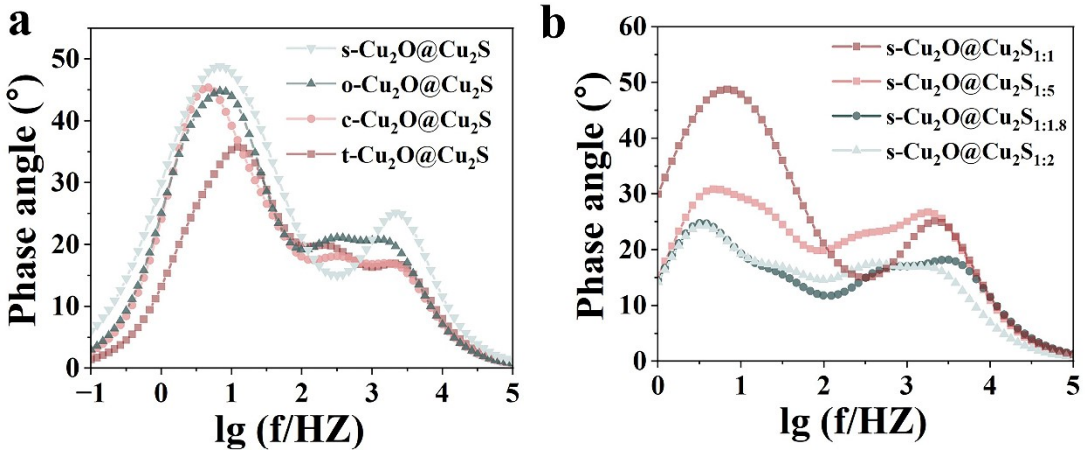

Fig. S9 Bode plots of several catalysts employed at -0.62 V vs. RHE.

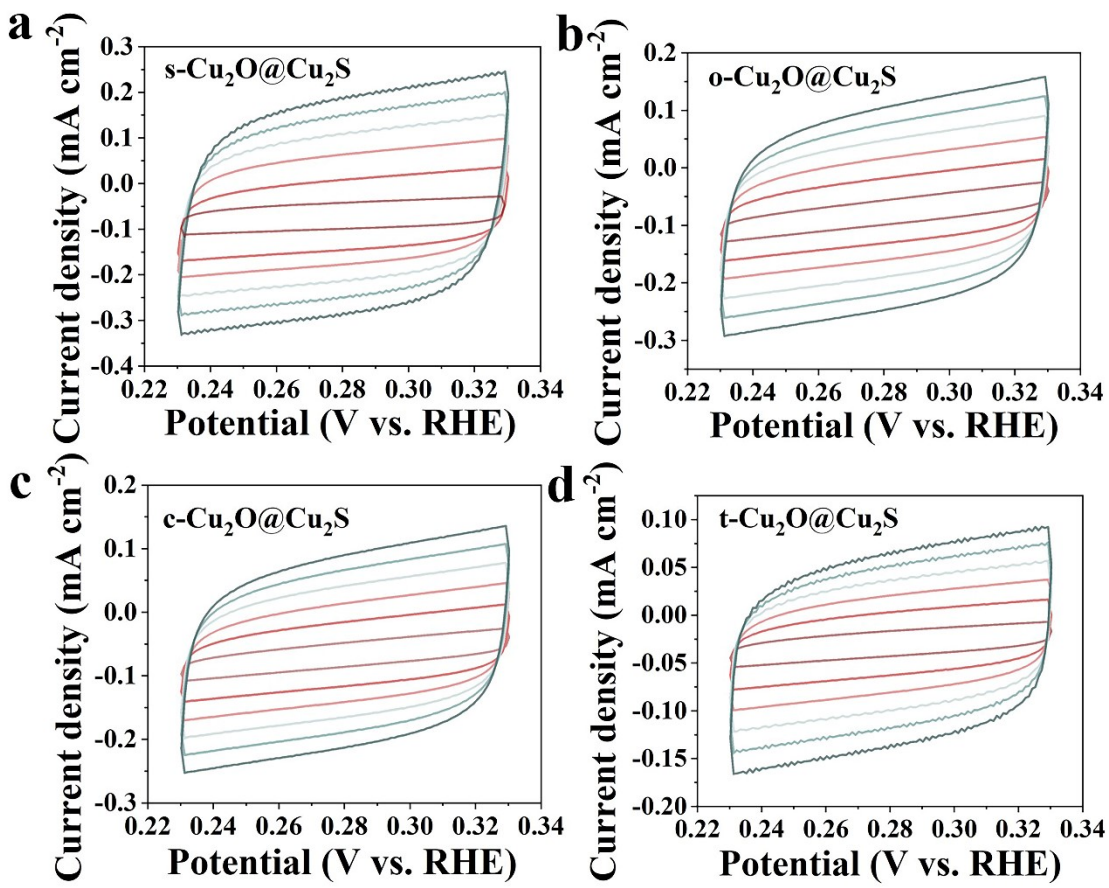

Fig. S10 CV measured at different scan rate from 10 to 100 mV s^{-1} in 0.5 M $KHCO_3$ for a) s-Cu_2O@Cu_2S, b) o-Cu_2O@Cu_2S, c) c-Cu_2O@Cu_2S, d) t-Cu_2O@Cu_2S.

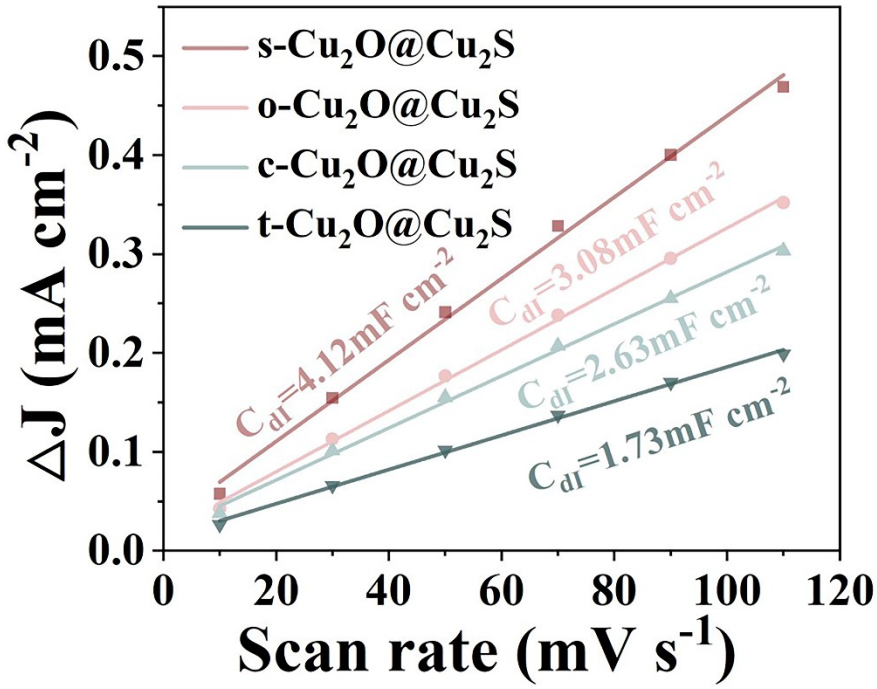

Fig. S11 The calculated C_{dl} value for the above electrocatalysts.

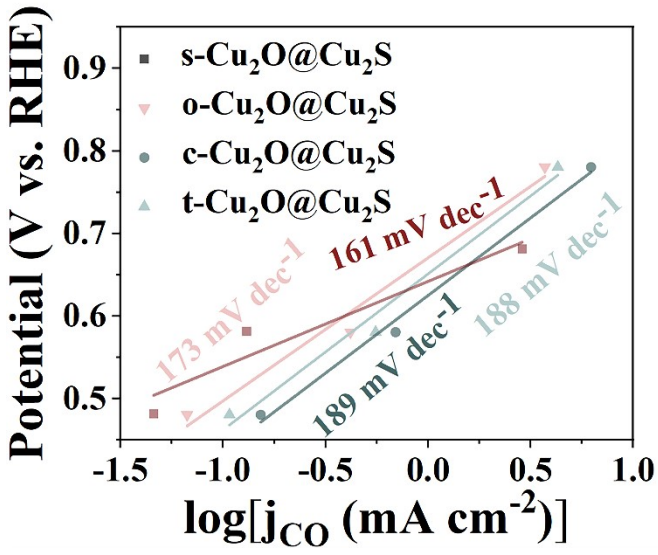

Fig. S12 Tafel slope of CO on a series of $Cu_2O@Cu_2S$ catalysts with different exposed crystal facet.

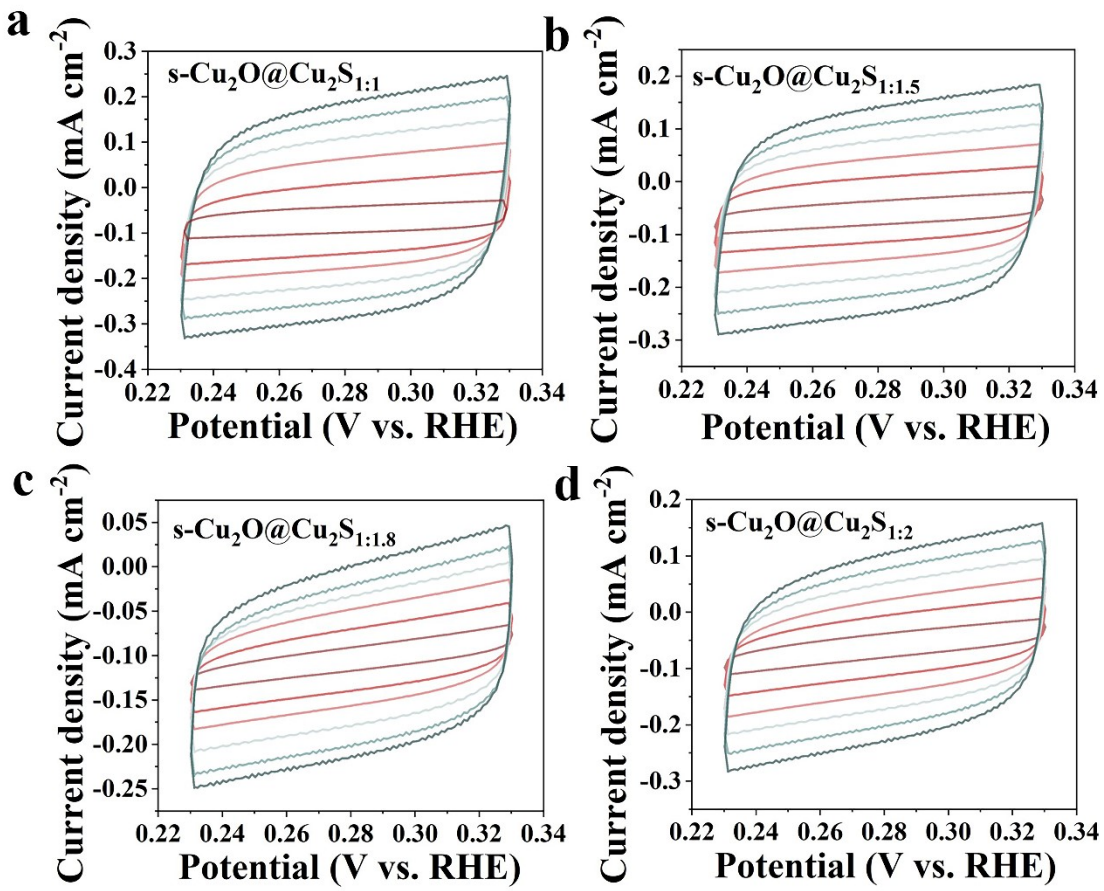

Fig. S13 CV measured at different scan rate from 10 to 100 mV s^{-1} in 0.5 M $KHCO_3$ for a) s-Cu_2O@$Cu_2S_{1:1}$, b) s-Cu_2O@$Cu_2S_{1:1.5}$, c) s-Cu_2O@$Cu_2S_{1:1.8}$, d) s-Cu_2O@$Cu_2S_{1:2}$.

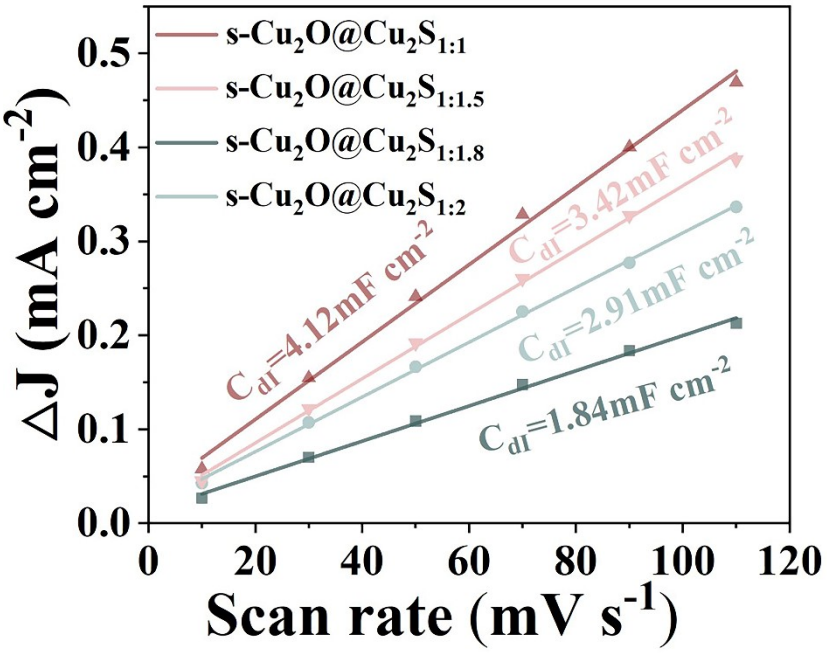

Fig. S14 The calculated C_{dl} value for the above electrocatalysts.

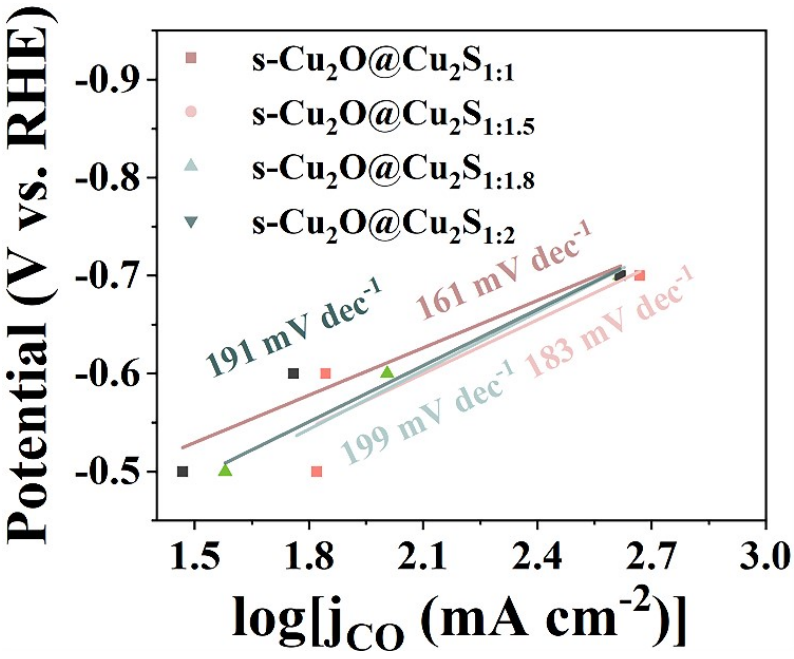

Fig. S15 Tafel slope of CO on s-Cu_2O@Cu_2S with varying sulfide layer thicknesses catalysts.

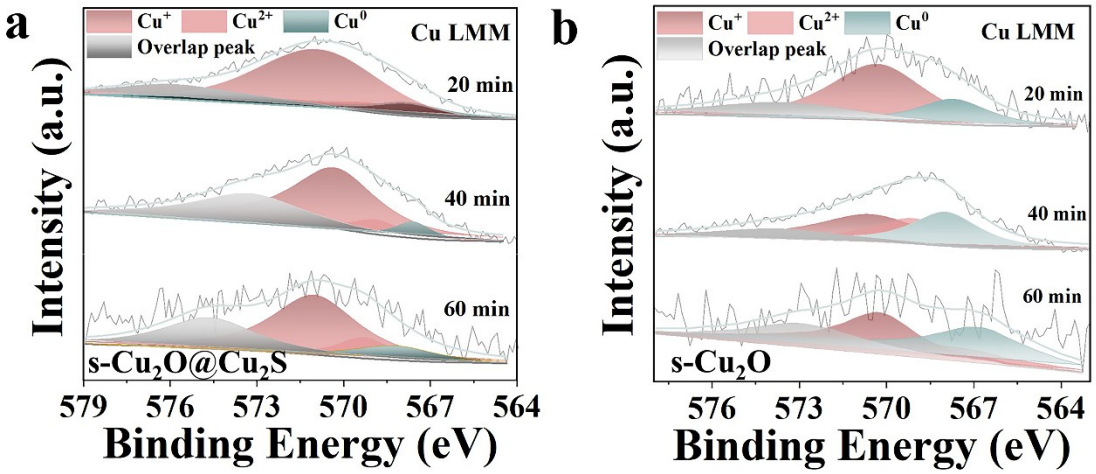

Fig. S16 Time-dependent Cu LMM Auger spectra for (a) s-Cu_2O@Cu_2S and (b) s-Cu_2O electrocatalyst from 20-60 mins electrolysis at -0.82 V vs RHE.

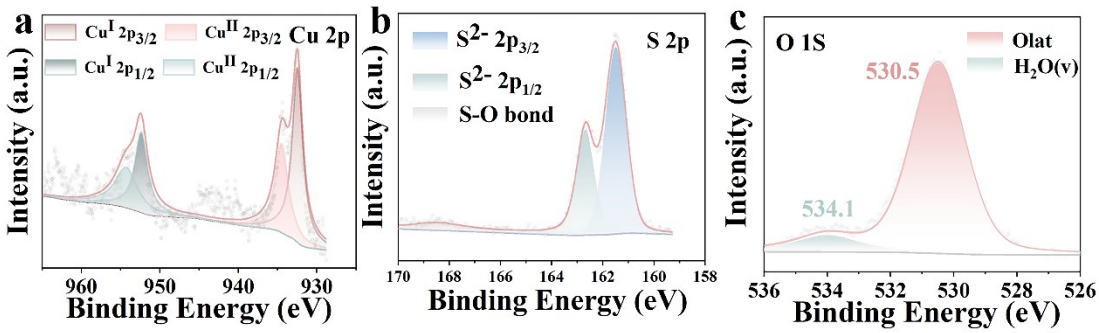

Fig. S17 Time-dependent XPS spectra collected from s-Cu_2O@Cu_2S samples of (a) Cu 2p; (b) S 2p; and (c) O 1s spectra for during 1 h electrolysis at -0.82 V vs RHE.

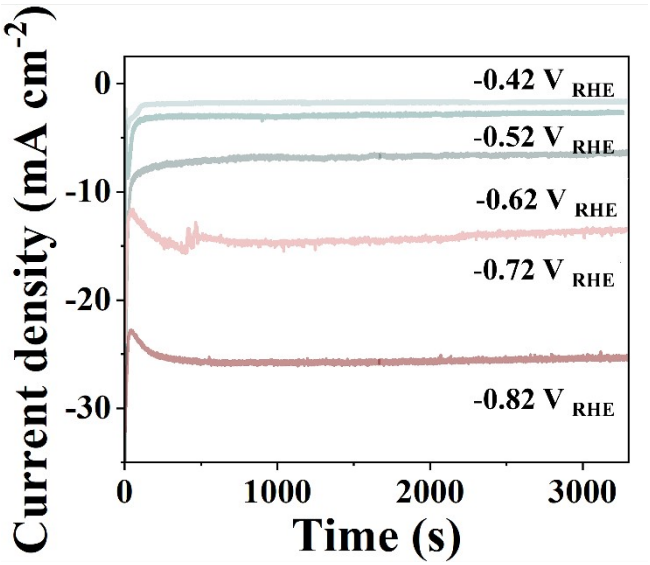

Fig. S18 Chronoamperometry curves of ECO_2RR over s-Cu_2O@Cu_2S in 0.5 M $KHCO_3$ solution at different potentials.

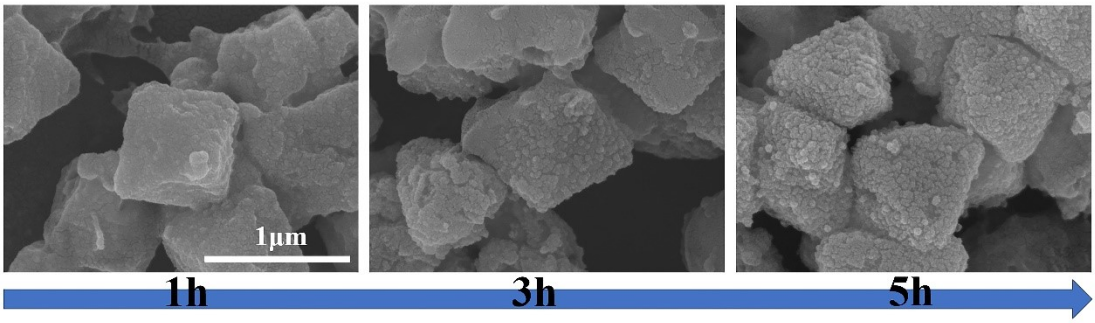

Fig. S19 SEM images captured the dynamic structural evolution process for o-Cu_2O@Cu_2S electrocatalysts.

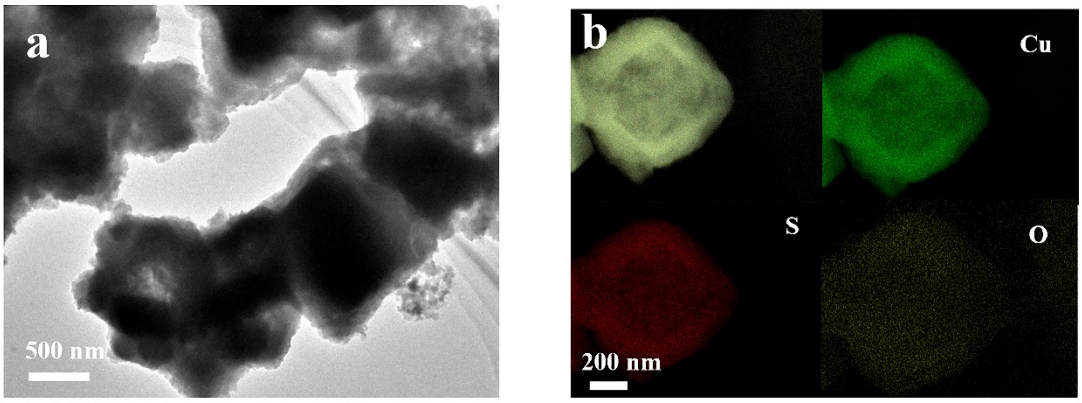

Fig. S20 (a) TEM image of the s-Cu_2O@Cu_2S sample, and (b) corresponding EDX elemental mapping images of Cu, S, and O in the s-Cu_2O@Cu_2S sample after electrolysis at -0.62 V vs RHE in CO_2 saturated 0.5 M $KHCO_3$.

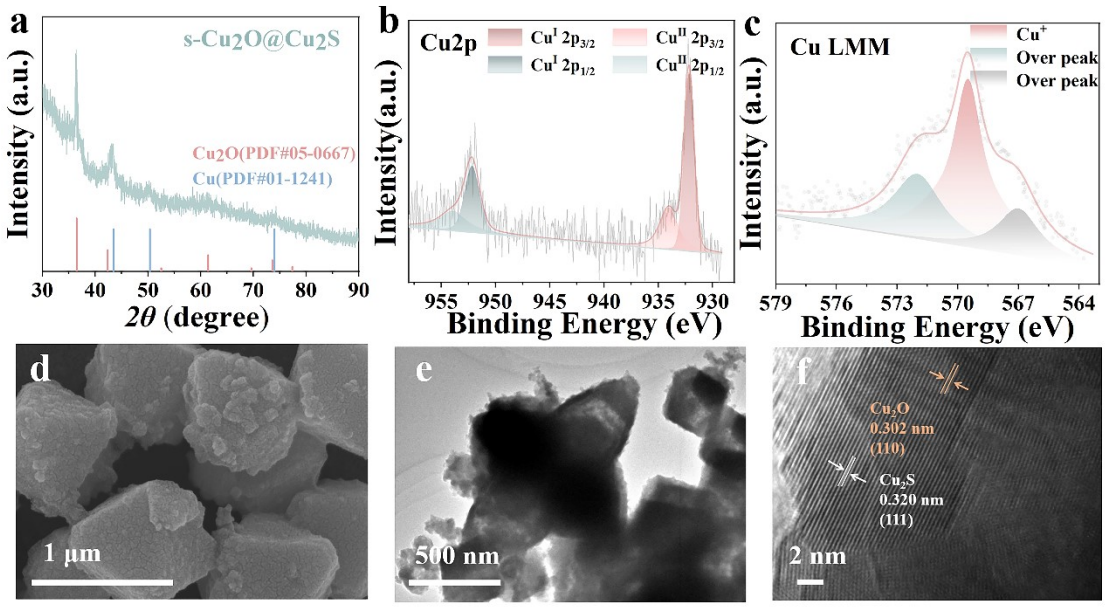

Fig. S21 (a) XRD patterns; XPS spectra of (b) Cu 2p; and (c) Cu LMM; (d) SEM image; (e) TEM image; and (f) HRTEM image of the s-Cu_2O@Cu_2S sample after 23 h electrolysis at -0.62 V vs RHE in CO_2 saturated 0.5 M $KHCO_3$.

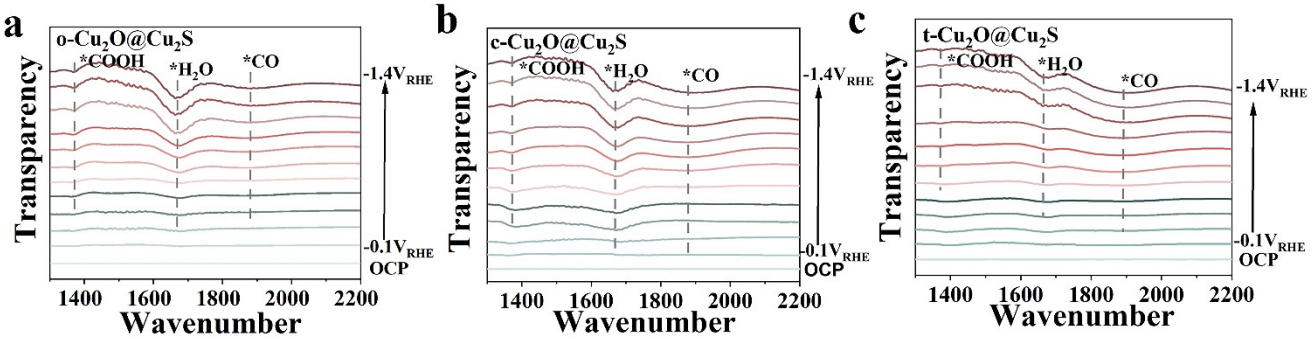

Fig. S22 (a) ATR-IR spectra recorded during stepping the potential from -0.1 V to -1.4 V on o-Cu_2O@Cu_2S, c-Cu_2O@Cu_2S and t-Cu_2O@Cu_2S in the solution containing 0.5 M $KHCO_3$ saturated with CO_2.

Table S1 Other advanced Cu and Cu_2O based electrocatalysts for CO_2 electroreduction to carbon monoxide.

Catalyst	Electrolyte	FE_{CO} (%)	E vs. RHE (V)	J_{CO} (mA cm^{-2})	Ref.
CuCo	0.5M ([Bmim]PF_6	97.4	-1.5	62.1	[1]
Sb-Cu	0.1M $KHCO_3$	82	-1.1	5	[2]
CuO/$In(OH)_3$-CNT	0.1M $KHCO_3$	89	-1.0	10.1	[3]
Cu-N - C	0.1M $KHCO_3$	89	-0.7	3	[4]
Cu_2Sb NA/CF	0.1M $KHCO_3$	86.5	-0.9	6	[5]
NiCux	0.1M $KHCO_3$	88.5	-1.0	13	[6]
Cu/ZnO	0.1M $KHCO_3$	94	-1.3v	11	[7]
CuPOFBpy/Cu_2O@CNT	0.5M $KHCO_3$	55	-0.9	-	[8]
s-Cu_2O@Cu_2S	0.5M $KHCO_3$	85	-0.62	7.5	This work

References

1. W. Guo, J. Bi, Q. Zhu, J. Ma, G. Yang, H. Wu, X. Sun and B. Han, Acs Sustain Chem Eng., 2020, **8**, 12561-12567.
2. H. Li, T.-W. Jiang, X. Qin, J. Chen, X.-Y. Ma, K. Jiang, X.-G. Zhang and W.-B. Cai, ACS Catal.., 2021, **11**, 6846-6856.
3. W. Li, Y. Yang, Z. Weng and S. Huo, J. CO_2 Util., 2021, **46**, 101470.

4. M. S. T. Song, M. S. Y. Wang, Z. Yuan, H. Liu, B. S. X. Zhang, B. S. L. Cui, B. S. Y. Chen, T. Liu and X. Zhang, ChemistrySelect., 2024, **9**, e202304917.
5. S. Mou, Y. Li, L. Yue, J. Liang, Y. Luo, Q. Liu, T. Li, S. Lu, A. M. Asiri, X. Xiong, D. Ma and X. Sun, Nano Res., 2021, **14**, 2831-2836.
6. C. Xu, A. Vasileff, B. Jin, D. Wang, H. Xu, Y. Zheng and S.-Z. Qiao, ChemComm., 2020, **56**, 11275-11278.
7. L. Xue, C. Zhang, T. Shi, S. Liu, H. Zhang, M. Sun, F. Liu, Y. Liu, Y. Wang, X. Gu and S. Zeng, Chem. Eng. J., 2023, **452**, 139701.
8. Q. He, H. Li, Z. Hu, L. Lei, D. Wang and T. T. Li, Angew. Chem. Int. Ed., 2024, **63**, e202407090.